Imaging Inward and Outward Trafficking of Gold Nanoparticles in Whole Animals

Valentina Marchesano,[†] Yulan Hernandez,[‡] Willi Salvenmoser,[§] Alfredo Ambrosone,[†] Angela Tino,[†] Bert Hobmayer,[§] Jesus M de la Fuente,[‡] and Claudia Tortiglione[†,*]

[†]Istituto di Cibernetica "E.Caianiello", Consiglio Nazionale delle Ricerche, Via Campi Flegrei, 34, 80078, Pozzuoli, Italy, [‡]Instituto de Nanociencia de Aragon, University of Zaragoza, C/Mariano Esquillor s/n, Zaragoza, Spain, and [§]Institute of Zoology, University of Innsbruck, A-6020 Innsbruck, Austria

ABSTRACT Gold nanoparticles have emerged as novel safe and biocompatible tools for manifold applications, including biological imaging, clinical diagnostics, and therapeutics. The understanding of the mechanisms governing their interaction with living systems may help the design and development of new platforms for nanomedicine. Here we characterized the dynamics and kinetics of the events underlying the interaction of gold nanoparticles with a living organism, from the first interaction nanoparticle/cell membrane, to the intracellular trafficking and final extracellular clearance. By treating a simple water invertebrate (the cnidarian *Hydra* polyp) with functionalized gold nanoparticles, multiple inward and outward routes were imaged by ultrastructural analyses, including exosomes as novel undescribed carriers to shuttle the nanoparticles in and out the cells. From the time course imaging a highly dynamic picture emerged in which nanoparticles are rapidly internalized (from 30 min onward), recruited into vacuoles/endosome (24 h onward), which then fuse, compact and sort out the internalized material either to storage vacuoles or to late-endosome/lysosomes, determining almost complete clearance within 48 h from challenging. Beside classical routes, new portals of entry/exit were captured, including exosome-like structures as novel undescribed nanoparticle shuttles. The conservation of the endocytic/secretory machinery through evolution extends the value of our finding to mammalian systems providing dynamics and kinetics clues to take into account when designing nanomaterials to interface with biological entities.

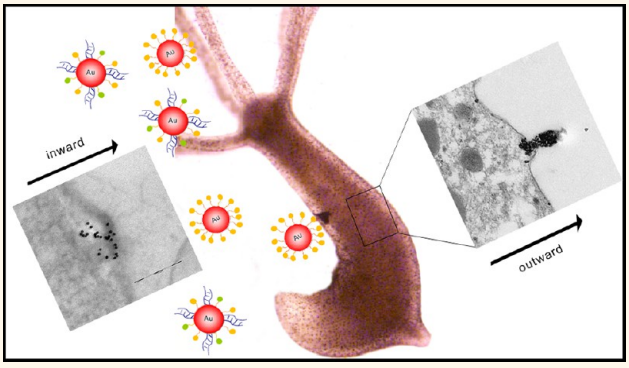

KEYWORDS: gold nanoparticles · cell uptake · intracellular trafficking · exocytosis · transmission electron microscopy · model organism · Hydra

The plasma membrane is a dynamic structure that functions to separate the cytoplasm from the extracellular environment by regulating and coordinating the entry and exit of small and large molecules. Small molecules, such as amino acids, sugars, and ions, can traverse the plasma membrane through the action of integral membrane protein pumps or channels. Macromolecules must be carried into the cell in membrane-bound vesicles derived by the invagination and pinching-off of pieces of the plasma membrane in a process termed endocytosis. The endocytic pathways (phagocytosis, (macro)pynocitosis) differ with regards to the size of the endocytic vesicle and the chemistry of the cargo triggering either membrane proteins (hormone mediated-signal transduction, cell–cell communication, immune surveillance, cell motility)[1] or cytosolic compartments. Within the endosome the cargos are sorted to distinct destinations, being either recycled back to the plasma membrane or sorted into intraluminal vesicles for lysosomal destruction *via* multivesicular bodies.[2] The macromolecular nature of the material transported by endocytosis makes this route one of the most important targets for nanomedicine.[3–5] Indeed, many nanoparticle formulations are customized to bypass cell membranes and deliver the cargo within the cell.[6–8] However, not much is known about the intracellular trafficking and fate of nanomaterials following cargo delivery,[9,10] and only a few studies report on their whole

* Address correspondence to c.tortiglione@cib.na.cnr.it.

Received for review December 13, 2012 and accepted March 1, 2013.

Published online March 01, 2013
10.1021/nn305747e

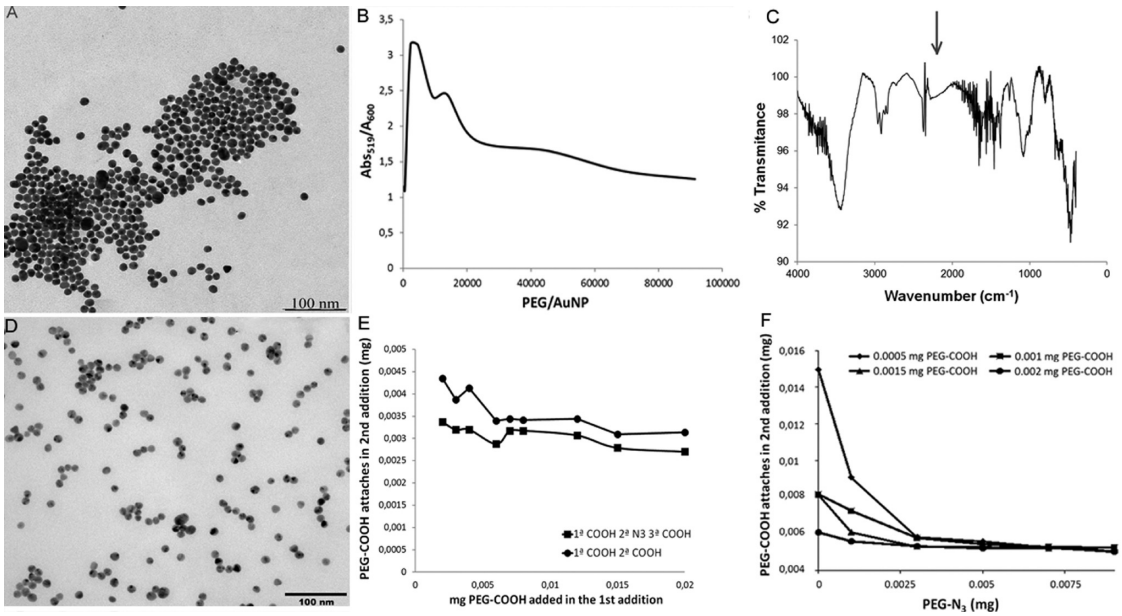

Figure 1. Characterization of AuNPs. The high monodispersity of the gold core of AuNP-N_3 (A) and AuNP-siRNA (D) was confirmed by transmission electron microscopy (TEM, T20 200KeV; FEI) showing an average size of 14 nm. (B) Analysis of the stability of AuNP-N_3: the ratio A519 (contribution of stable AuNPs)/A600 (contribution of aggregated AuNPs) was measured by UV−vis. (C) Infrared spectra (FTIR, JASCO FT/IR 4100) confirmed the presence of the azide groups covering the gold cores, showing a characteristic peak at 2100 cm^{-1}. Quantification by Ellman's method of the PEG-COOH chains attached in a second addition after (E) increasing amount of PEG-COOH with (squares) and without (circles) PEG-N_3, (F) increasing amount of PEG-N_3 at constant PEG-COOH added. Data were collected from a single experiment, developed by J. Conde during previous work.[25] Whole characterization of AuNP-siRNA has been extensively reported.[25]

journey into the cell up to external clearance. Gold nanoparticles (AuNPs) hold great interest in this field thanks to properties such as monodispersity, stability, minimal toxicity, excellent contrasting agent properties for transmission electron microscopy (TEM) analysis, which enable to track with unprecedented resolution dynamic of uptake, intracellular sorting, and potential secretion.[11−13] Recent results gathered on the interaction of AuNP with different synthetic lipid membranes[14] or cell lines demonstrated that properties such size, charge, chemical functionalities, but also the arrangement of organic ligands on nanoparticle surface, dictate the internalization route.[15,16] Moreover, surface functionalization may influence the fate of AuNP upon cell uptake: HUVEC cells treated with AuNP coated by different peptides display distinct exocytosis profiles.[9] Here we investigated the inward and outward trafficking of AuNPs at whole animal level using the small invertebrate *Hydra vulgaris* (Cnidaria, Hydrozoa), a recently emerged amenable system to study nanoparticle−cell interactions.[17,18] Shaped like a simple hollow cylinder with a single apical opening (mouth) surrounded by a tentacle crown and a basal foot to anchor a substrate (Figure 2B).[19] *Hydra* is a freshwater polyp successfully used to test diverse nanoparticles, for example, for evaluation of toxicity of CdTe quantum dots,[20,21] to study cell dynamics using fluorescent quantum rods,[22] or to analyze animal behavior in response to nanoparticle exposure.[23] The possibility to uniformly expose the whole animal to any given substance by simple soaking makes it ideal to study the mechanism of nanoparticle uptake and fate. In fact, the tissue structure, organized as just two cell layers (ectoderm and endoderm) facing respectively the animal external side and the gastric cavity, enables us to finely track NPs interaction with *Hydra* cells upon pulsed or prolonged exposure at any desired time point. We have recently shown that the capability of *Hydra* cells to uptake soluble macromolecules is greatly enhanced by the positive net charge. CdSe/CdS poly(ethylene glycol) (PEG) coated quantum rods, displaying negative zeta potential as-synthesized, under the condition of charge reversal (*i.e.*, acidic pH) acquire positive charge and capability to enter *Hydra* cells at high efficiency.[22] Similarly, short dsRNA, if protonated at acidic pH, are uptaken at a high rate into the cytosol and are able to initiate an RNAi response,[24] showing the pivotal role played by the positive charge in enhancing cell permeability to several structures, chemically unrelated. Our group has recently shown that multifunctional gold nanoparticles, stabilized by PEG and conjugated to several bioactive molecules (siRNA, TAT, charged groups) are capable of cytosol delivery of small interfering RNAs (siRNA) and induction of a specific RNAi process.[25] The selected siRNA targeted the proto-oncogene *c-myc*, a key gene controlling disparate aspects of cell physiology including cell growth, cell cycle progression, biosynthetic metabolism, and apoptosis and, as expected, found deregulated in the majority of human cancers. Remarkably, these multifunctional

myc-siRNA AuNPs induced specific and efficient RNAi in three different biological systems (human cell culture, *Hydra*, and mouse) thus representing a broadly valid nanotool to achieve gene silencing. In *Hydra* the downregulation of the myc gene (previously isolated by Hartl *et al.*[26]) mediated by myc-siRNA-AuNP induced 80% downregulation[25] and the same effects caused by free siRNA,[24] confirming the specificity of the new approach. Briefly, *Hymyc1* inhibition caused increased proliferation of interstitial stem cells, suggesting a role in maintaining the balance between stem cells self-renewal and differentiation, as found in other systems. Ultrastructural analysis by TEM showed the capability of myc-siRNA nanostructures to directly penetrate *Hydra* cell membranes,[25] while in human cells and mouse lungs classic endocytic routes were found. Considering the broad potential of the new nanotool to enter RNAi-based clinical trials, basic knowledge of the rule governing the interaction of such smart nanoparticles with a cell membrane is of fundamental importance, together with the understanding of kinetics of the gold clearance following siRNA delivery. To get deep insights on these mechanisms, here we used an ultrastructural approach to analyze all steps of AuNP cell/interaction using the *Hydra* model. By comparing different chemical functionalities (siRNA and positively charged groups), administration dose, and incubation times we identified novel inward and outward routes, capturing for the first time at whole animal level AuNP exocytosis. The strong evolutionary conservation of the endocytic/secreting machinery in the animal kingdom makes our findings of broad value not only for nanomedicine/pharmacological aims, but also to unravel, *in vivo*, basic mechanisms and parameters regulating cell portals of entry, negotiation, and secretion.

RESULTS AND DISCUSSION

Synthesis and Surface Modification of Gold Nanoparticles. Two types of AuNPs were employed in this study: surface-modified by azide group (AuNP-N_3) and by siRNA targeting the c-myc gene (AuNP-siRNA). AuNPs used as starting material for both functionalizations were synthesized following the straightforward methodology reported.[27] The obtained AuNPs had an average size of 14 nm (Figure 1A,D). Citrate protective layer was exchanged by a hepta-ethylenglycol spacer including a thiol and an azide functional groups. Thiol moiety was used to react with Au atoms of the AuNP and to establish a strong Au−S pseudo-covalent bond. The azide group was incorporated for further functionalization of the nanoparticles by "click chemistry" reactions with alkyne moieties (data not shown). Moreover, surface modification with PEG resulted in prolonged stability of the nanoparticles in the animal growing media, minimizing unwanted aspecific protein interactions and decreased toxicity of the nanoparticles. Removal of citrate groups from the surface of the nanoparticle caused changes of Z potential changes, from −38 mV to +21 mV, which could drastically modify the cellular uptake. The best conditions for obtaining stable and derivatized AuNPs were obtained by adding different AuNP/PEG-N_3 ratios. The most stable nanoparticles were obtained with AuNP/PEG-N_3 ratios between 1:2000 and 1:5000, and around 2600 PEG-N_3 chains/AuNP were estimated at the maximum point. The addition of higher or lower amounts of PEG-N_3 decreased drastically the stability of nanoparticles (Figure 1B). The presence of N_3 moieties on the AuNP surface was proved by FTIR analysis (Fourier transform infrared spectroscopy), showing a characteristic peak at 2100 cm^{-1} (Figure 1C). MALDI TOF of AuNP-N_3 further confirmed the presence of PEG-N_3 ($M-H^+$ 451.1). In the case of the AuNPs-siRNA, the functionalization was made as previously described,[25] decreasing the total amount of PEG for further incorporation of thiolated siRNAs. To overcome the low stability of partially pegylated nanoparticles using PEG-N_3 chains, 50% of carboxylated PEG chains was added. Quantification of PEG-COOH and PEG-N_3 chains bound to AuNPs was performed as previously reported.[25] Briefly, PEG-COOH chains were measured directly by the determination of the excess of thiol groups in supernatant by Ellman's method, while in the case of PEG-N_3 chains, an indirect methodology was designed. An accurate description of the quantification of degree of saturation for the PEG chains on AuNP is reported in ref 25, and the results shown in Figure 1E,F. The number of PEG chains on AuNP-siRNA was estimated as 1250.5 ± 279.8. The addition of siRNA also improved the stability of the AuNP due to their negative charge.[28] Quantification of myc siRNA strands following covalent binding to AuNPs (see Material and Methods) led to estimate 41.3 ± 0.8 siRNA strands loaded on AuNPs. The addition of siRNA on NP surface causes a zeta potential switch toward negative values like −25.5 ± 1.2 mV. In Table 1 a summary of the AuNP features is reported, while a scheme of the structure of two nanoparticles is shown in Figure 2 panels A and H.

TABLE 1. Quantification of the PEG Chains, and siRNA Strands for AuNP-N_3 and AuNP-siRNA Bioconjugates, Together with the Z-Potential and Dynamic Light Scattering (DLS) Measurements

AuNP conjugate	PEG chains/NP	siRNA strands/NP	zeta potential (mV)	DLS (nm)
AuNP-N_3	∼2600		+21	15.5
AuNP-siRNA	1250.5 ± 279.8	41.3 ± 0.8	−25.5 ± 1.2	138.7

Influence of Surface Chemistry on NP Uptake: Biodistribution and Ultrastructural Analysis of AuNP-siRNA and AuNP-N_3. A preliminary toxicological evaluation was performed to ensure the absence of harmful effects elicited by AuNPs treatments. Living polyps were soaked 24 h with

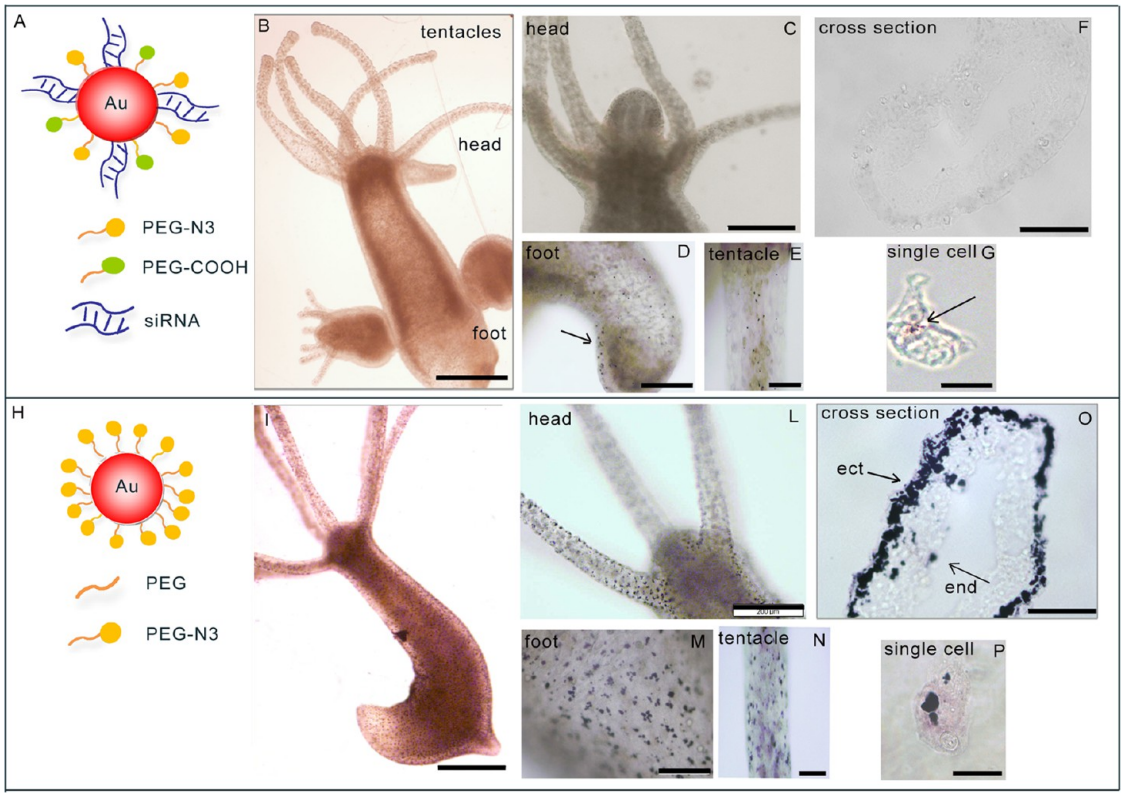

Figure 2. ***In vivo*** **uptake and biodistribution of AuNPs in** ***Hydra*****. Upper panel: interaction of** ***Hydra*** **with AuNP-siRNA. (A) Schematic illustration of the AuNP-siRNA shows the nanoparticle structure, coated by two different PEG spacers (PEG-COOH, and PEG-N_3), and functionalized with siRNA molecules.[25] (B) Bright field image of a living** ***Hydra*****, carrying two developing buds, treated 24 h with AuNP-siRNA. Internalized nanoparticles are hardly detectable by whole animal imaging. Zooming into (C) head, (D) foot, and (E) tentacle regions shows nanoparticles as dark granules located on ectodermal cells; (F) tissue cryosections prepared from treated animals. AuNPs are not detectable on such preparation, while (G) single cells preparations AuNPs are visible (arrowed) into the cytosol of ectodermal cells. Scale bars: (B) 500 μm; (C,F,D) 200 μm; (E) 100 μm; (G) 50 μm. Lower panel: Interaction of** ***Hydra*** **with AuNP-N_3. (H) Nanoparticle scheme illustrating the homogeneous PEG-azide coating the Au core. (I) A strong punctuated dark labeling is present uniformly all over animal. The pattern is clearly evident on separate imaging of (L) head, (M) foot, and (N) tentacles of treated polyps. (O) Cryosections from labeled polyps show massive AuNP-N_3 accumulation into the ectoderm (ect) and the endoderm (end). (P) Fixed single cell suspension reveals AuNP-N_3 location into vesicle-like structures of different sizes. Scale bars: (I) 500 μm; (L,O,M) 200 μm; (N) 100 μm; (P) 50 μm.**

70 nM AuNP-siRNA, a concentration previously shown to induce efficient gene silencing[25] and with the same amount of AuNP-N_3. Polyp morphology was not affected by NP exposure, neither their reproductive capability, as shown by the growth rates of treated animals, not significantly different from control untreated animals (Supporting Information, Figure S1). The bright field images of Figure 2 show a weak punctuated labeling pattern over the body and tentacles (Figure 2D,E), confirming a low rate of internalization of AuNP-siRNA. These NPs were not detectable on cryosections prepared from treated polyps (Figure 2F) while on single cell suspensions a pink colored labeling was found on a small percentage of cells (Figure 2G). Polyp treatment with AuNP-N_3, by contrast, produced a strong punctuated labeling all over the animals (head, body, and tentacles) (see Figure 2 I–N). Cryosections of treated specimens (Figure 2O) showed internalized AuNP-N_3 both within the ectoderm and few endodermal cells, confirming previous evidence on dynamic processes occurring between the two cell epithelia, causing displacement or migration of labeled cells or free NPs from the ectoderm to the endoderm.[22] Single cell analysis confirmed the localization of these AuNPs into large cytoplasmic structures (Figure 2P). To investigate the mechanisms underlying this different internalization efficiency, polyps were incubated for increasing periods (5 min, 30 min, and 24 h) with both AuNP types before processing for TEM analysis.

AuNP-siRNA Cell Uptake Dynamics. While a short incubation time (5 min) was not sufficient to detect AuNP-siRNA (Figure 3A), the first clear interactions between AuNP-siRNA and the cell membrane was detected after 30 min of incubation. At this time point (Figure 3B,C) AuNP-siRNA are found very close to the cell membrane and also in the act of passing through it, indicating the capability of AuNP-siRNA to directly penetrate the plasma membrane of *Hydra* ectodermal cells. While most of the literature data report on the endocytic-endolysosomal pathway as the main route mediating the entry and fate of NP inside the cells (and often

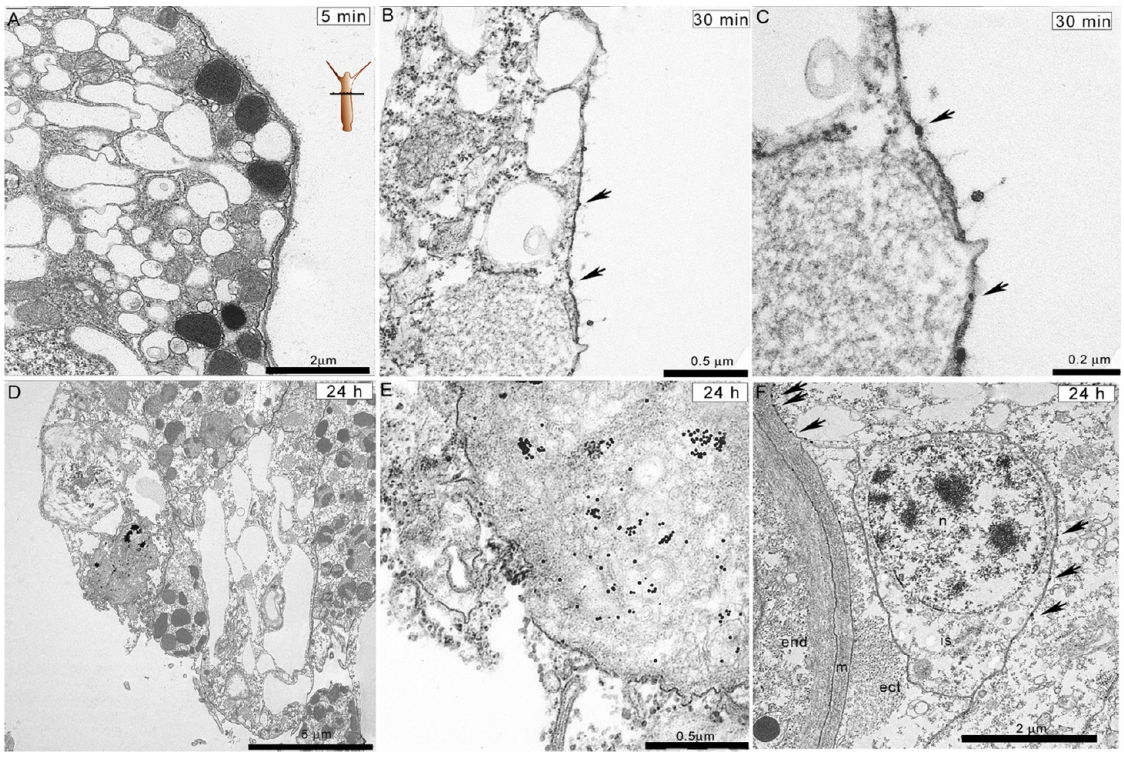

Figure 3. Ultrastructural analysis of AuNP-siRNA uptake. Polyps were treated with AuNP-siRNA for (A) 5 min, (B,C) 30 min, (D−F) 24 h, then carefully washed and processed for TEM. Thin sections were obtained cutting the animal at the mid gastric or subhypostomal (below the mouth) level, as shown schematically in the upper part of image A. After 5 min, the first interactions between AuNP and *Hydra* membranes are not detectable, while after 30 min, at higher magnification (B and C), single NPs or clusters of 2−3 units are detected in close proximity of the plasma membrane or within it (indicated by black arrows). In panels D and E images at increasing magnification show AuNP-siRNA located within a dense cytosol region, likely representing a lysosome. In this environment, NPs are not degraded. (F) AuNP-siRNA are detected after 24 h of incubation on the membrane of interstitial cells (is). This single stem cell is located in the interstices between ectodermal cells close to the mesoglea (m), which separates ectoderm (ect) from the endoderm (end). AuNP-siRNA are found also on the mesoglea, indicating the capability of the NP to reach several tissue districts from the original ectodermal delivery. Scale bars: (A) 2 μM; (B) 0.5 μM; (C) 0.2 μM; (D) 5 μM; (E) 0.5 μM; (F) 2 μM.

limiting the cytoplasmic delivery),[29] the direct passage of the gold nanoparticle through the cell membrane has been rarely reported, and in a few cases has been associated to the ordered surface structure.[30,31] TEM analysis performed after 24 h of incubation detected AuNP-siRNA within a dense cytosol region. Figure 3D,E show free nanoparticles or as clusters of a few units within a dense region of an ectodermal cell, likely representing a late endosome. Interestingly, AuNP-siRNA were also found on membranes of interstitial cells, laying in the interstices between ectodermal cells, proving the capability of NP to freely traverse cell layers, delivering their siRNA cargo far from the administration site (Figure 3F).

AuNP-N_3 Cell Uptake Dynamics. A different dynamic of internalization emerged from the TEM analysis of AuNP-N_3 incubated over the same periods with *Hydra* polyps (Figure 4) at the same concentration (70 nM). Supporting Information, Figure S2 shows, after 5 min of incubation AuNP-N_3 bound to the glycocalix, a thick "cuticle layer" composed by glycoproteins and glycosaminoglycans, covering the animal's outer surface (Supporting Information, Figure S3). This molecular composition of this cuticle layer has been recently identified.[32] The strong interaction between the positive azide group of the AuNP and the negative cuticle components caused in 30 min the massive accumulation of nanoparticles all around the animal tissue. The ectoderm appeared as a typical scalloped surface with branching crypts extending into the epithelium between cells or groups of cells, uniformly labeled by electron dense material (Figure 4A). Interestingly, large vacuoles in the act of fusing/dividing (Figure 4A and Supporting Information, Figure S4) were often found in the apical part of the ectodermal cells, whose probable origin from membrane invagination and fusion (macropynocytosis) is indicated by the presence of the glycocalix/cuticle lining the inner side of the limiting membrane. Single AuNPs moving through the glycocalix to reach the cytoplasm revealed the dynamic state of such structures (Figure 4B, arrows). Remarkably, this phenomena has been recently described in HeLa cells incubated with TAT-modified AuNPs: ultrastructural analysis showed NPs to freely negotiate intracellular barriers, moving from vesicles to cytoplasm in either way by direct membrane translocation.[33] Our study

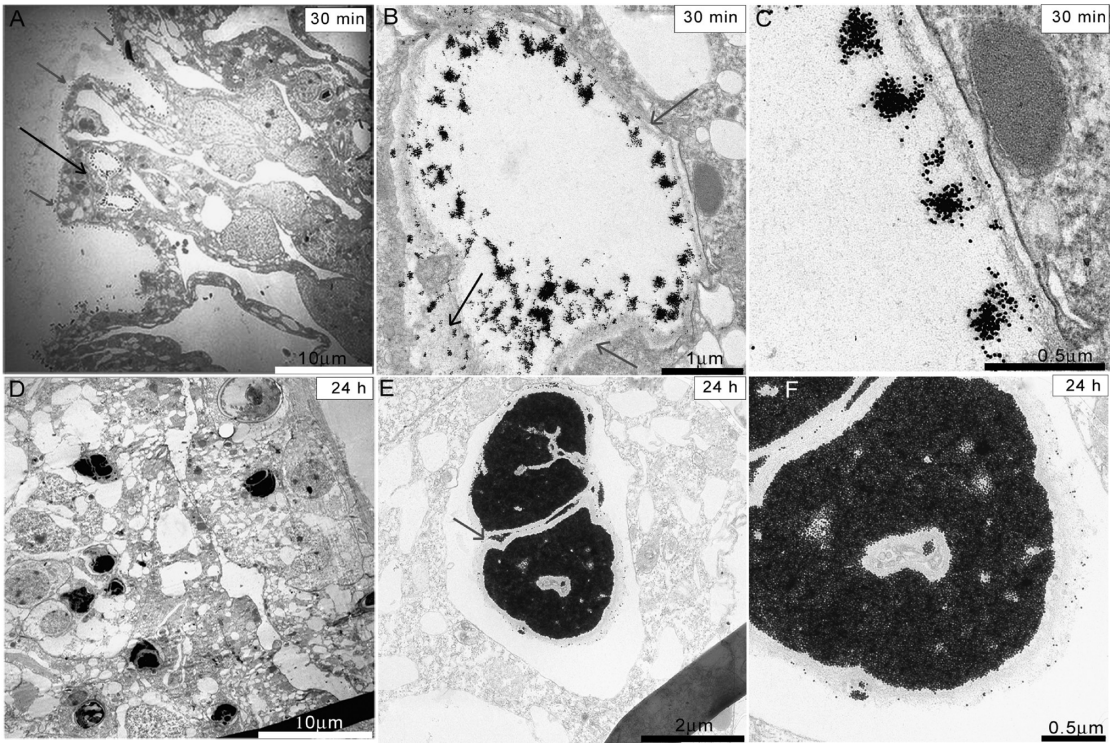

Figure 4. Ultrastructural analysis of AuNP-N_3 uptake. *Hydra* **polyps were exposed to AuNP-N_3 for (A−C) 30 min, (C−E) 24 h, then extensively washed and processed for TEM. (A) At 30 min time point, AuNP-N3 were found attached to the glycocalix, uniformly decorating the animal outer surface (gray arrows), but also inside large vacuoles (black arrow). (B) At higher magnifications the inner side of this structure appears lined by the glycocalix layer, proving the origin from membrane invagination (gray arrows). AuNP-N_3 are also captured coming out this structure (black arrow) by direct membrane translocation toward the cytosol. (C) A close view of the AuNP-N_3 entrapped into the vacuoles together with the glycocalix components. (D) At 24 h time point a massive accumulation of AuNP-N_3 into micrometer-sized vesicles is found. In images E and F, higher magnifications of such structures clarify the presence of membrane components in between the packed NPs, suggesting multiple self-fusion and invagination events. Scale bars: (A,D) 10 μM; (B) 1 μM; (C,F) 0.5 μM; (E) 2 μM.**

also shows AuNP-N_3 directly crossing intracellular or plasma membranes (Supporting Information, Figure S5), as observed with AuNP-siRNA, suggesting multiple mechanisms governing the permeability of cell membrane to AuNPs, and the possibility of identical routes for different chemical functionalities. The most intriguing finding was observed at the 24 h time point analysis (Figure 4D−F), where AuNP-N_3 were found massively packed into micrometer-sized granular structures, mixed to glycocalix/subcellular debris components. These structures, responsible for the punctuated pattern observed by optical microscopy (see Figure 2 I−P), may arise from inward budding of the membrane limiting the endosomal-like structures, as described in mammals.[2] The occurrence of self-folding and fusion events between multiple units may account for the presence of glycocalix components interspersed between the AuNP aggregates (Figure 4E,F). Similar vesicles densely packed by AuNPs have been described also in HeLa cells,[33] suggesting a conserved mechanism exploited by eukaryotic cells to sort out foreign material. In *Hydra* they may represent storage/garbage vacuoles, possibly due to the saturation of the lysosome machinery unable to sort out high NP concentration. The current view of endosome and lysosomes as dynamic organelles that repeatedly fuse each other and with cell membrane to either degrade, store, or secrete their content,[34] makes at this stage several hypothesis possible. Our ultrastructural analysis of AuNP-siRNA or AuNP-N_3 uptake indicates that the surface chemistry of the gold nanoparticles controls the efficiency of internalization but not the mechanism itself. The positive surface charge does mediate the intimate contact between the nanoparticles and the cuticle (due to high binding affinity) greatly enhancing, together with the high dose, the uptake. Following this initial interaction, the same mechanisms of entry into the cells can be exploited by both nanoparticle functionalizations, either through endocytosis (including macropynocytosis) or direct membrane translocation. The active/passive nature of the mechanism mediating NP penetration through the membrane and its dependence from the NP surface structure remains to be elucidated.

Ultrastructural Evidence of AuNP-N_3 Exocytosis. To get deeper insights into the events characterizing the uptake and fate of AuNP, we focused on AuNP-N_3, avoiding the potential effect played by additional biomolecules (size, structure, chemistry properties) on the uptake, and also because these NPs represent starting material for further functionalizations. A lower dose of AuNP-N_3

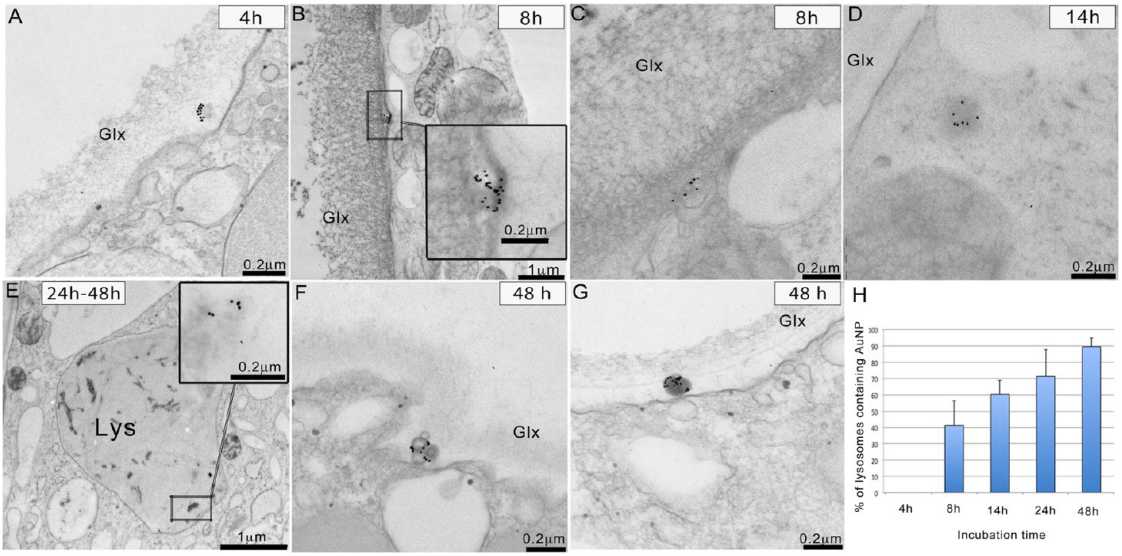

Figure 5. High-pressure cryo-TEM reveals additional internalization pathways. Time course analysis of AuNP-N_3 interaction with *Hydra vulgaris*. Polyps were incubated for the indicated periods with 25 nM AuNP-N_3. (A) Single distinguishable AuNP-N_3 appear attached to nanosized vesicles outside the cell membrane, within the glycocalix (Glx). (B) Later on the vesicles are found traversing the cell membrane (B,C) to reach (D) the cytoplasm. (E) At 24 and 48 h time point most of the AuNP-N_3 are detected inside lysosomes (Lys). (F,G) At 48 h nanosized vesicles loaded by NPs are also found outside the cell membrane. (H) An estimation of the lysosome containing NPs (expressed as percentage ± SE) shows that they increase from 8 to 24 h of incubation, when most of uptaken NPs are delivered to lysosomes for degradation. The estimation was done at each time point on 20 TEM images collected from three different animals. Scale bars: (A,C,D,F,G) 0.2 μM; (B,E) 1 μM.

was employed for animal treatment (25 nM) and the analysis, extended along a wider temporal window, performed by mean of high-pressure cryo-TEM, which avoids ice-crystal formation and potential fixative artifacts, enabling ultrastructural description as close as possible to the living state. In Figure 5, representative TEM images of a time course analysis (4−48 h) show after 4 h incubation the selective binding of the nanoparticles to dense material within the inner glycocalix layer, lining the round-shaped surface of a vesicle-like structure (Figure 5A). At 8 h these NP-decorated vesicles are found crossing the cell membrane (Figure 5B,C), reaching at 14 h time point the cytosol (Figure 5D). The cytosolic location of AuNP-N_3 decreases after longer incubation times. Indeed, at 24 and 48 h time points AuNP-N_3 were mainly found inside morphologically distinguishable lysosomes, as single units or small clusters (Figure 5E), indicating the lysosomal pathway as the main intracellular fate. By counting the NP-containing lysosomes, their percentage was found directly correlated to the increase of the incubation time, reaching 90% of the total analyzed lysosomes at 48 h (Figure 5H). Surprisingly, the finding at 48 h of nanozised vesicles loaded with NPs outside the cell membrane (Figure 5F) opened the possibility that beside their role as carriers of AuNP from the external medium inside the cell, they could also represent endosome recycled material brought back to the cell membrane. In mammals the fusion of multivesicular bodies with the cell membrane may induce the release of 30−100 nm sized exosomes into the extracellular space.[35,36] Extensive investigations at this time point performed on at least five different animals (and an average of 20 observations) confirmed AuNP-N_3 associated to dense nanovesicles laying just outside the plasma membrane. This material appears secreted by ectodermal cells, as indicated by the frequent presence of empty vesicles of identical size on the cytosolic side of the cell membrane (Figure 5G and Supporting Information, Figure S6). The occurrence of secretory events is suggested also by the cell membrane morphology, appearing interrupted at different sites due to the external release of nanovesicles (see Figure S6). To further confirm the exocytosis pathway, a "pulse and chase" experiment was carried out. Living animals were incubated for 24 h with AuNP-N_3, extensively washed, and incubated in fresh medium for a further 24 h and 48 h before processing for TEM and elemental analysis. TEM images in Figure 6 clearly reveal, 24 h postincubation, vesicles containing NP in the apical part of the cell (Figure 6A), on the glycocalix layer (Figure 6B), and in the act of being released outside the cell (Figure 6C). Other images captured exocytosis by the shedding of vesicles densely packed with AuNPs or mediated by multiple vesicle release through larger membrane areas (Figure 6D−F). As the lysosome content can be directly released outside the cells (Supporting Information, Figure S7A), we conclude that multiple pathways may be employed for AuNPs secretion. A hypothetical scheme summarizing our experimental findings is presented in Figure 7.

Elemental Analysis Confirms Kinetic of Uptake and Clearance of AuNP. To quantitatively estimate the amount of AuNP-N_3 internalized by *Hydra* and possibly the extent

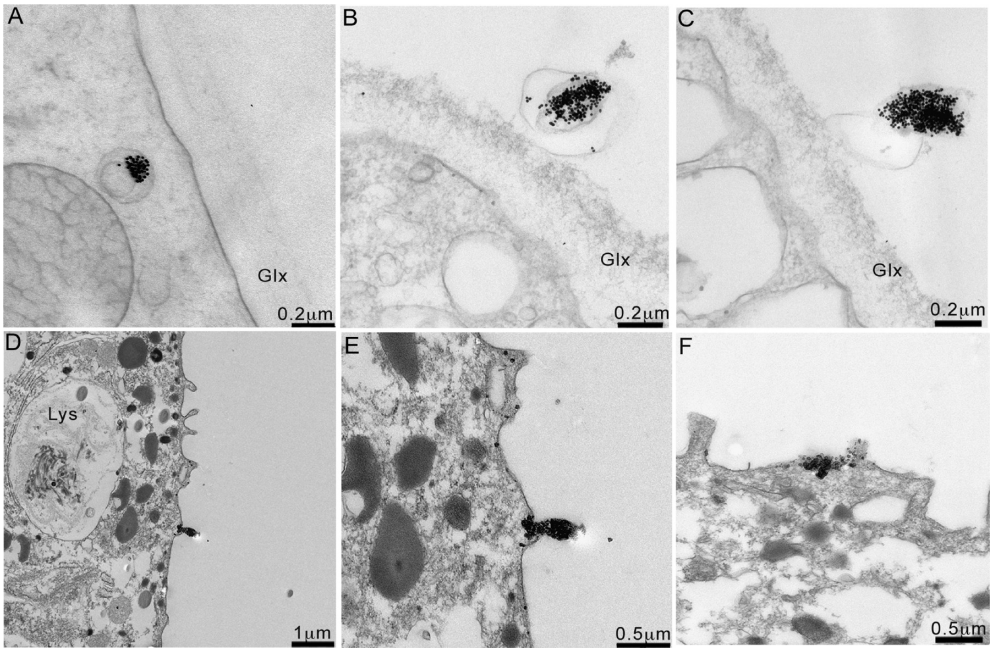

Figure 6. Exocytosis of AuNP-N_3. Polyps were "pulsed" 24 h with AuNP-N_3, extensively washed, and "chased" by incubation for additional 48 h in fresh medium, before processing for TEM analysis. (A) AuNP-N_3 are found on the apical part of the cell, entrapped into nanosized vesicles that are released out of the animal (B,C). In image D a low magnification image shows the whole animal tissue section in the act of AuNP-N_3 clearance. Other similar membrane shedding without NP are present on the animal surface, proving the normal occurrence of this phenomena. The same region at higher magnification is shown in image E. (F) Other tissue regions showing NP clearance. In this case a larger membrane area is involved, probably reflecting lysosome exocytosis. Scale bars: (A−C) 0.2 μM; (D) 1 μM; (E,F) 0.5 μM.

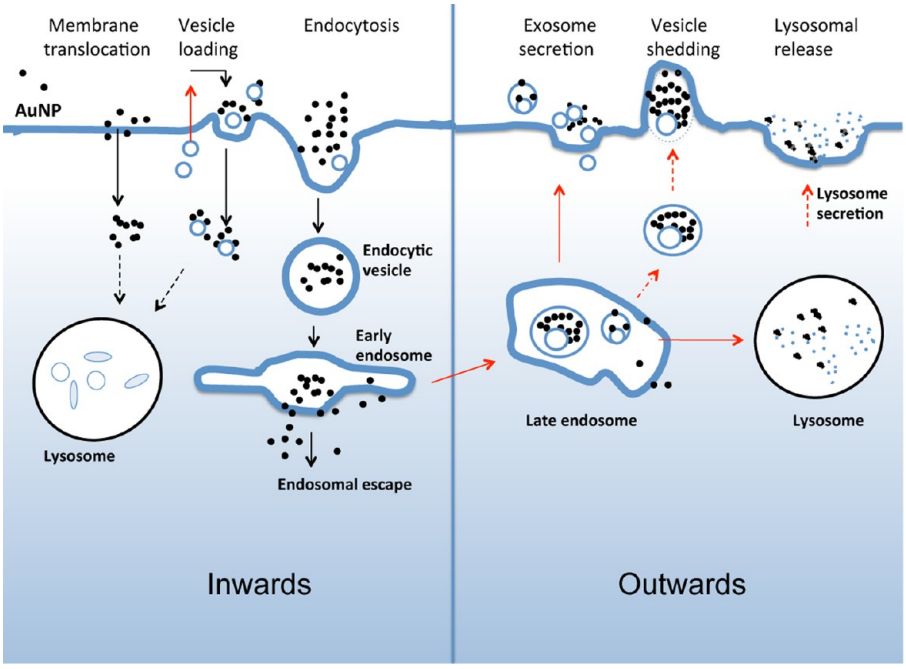

Figure 7. Schematic representation summarizing inward and outward trafficking routes of AuNPs. Following AuNP exposure to *Hydra*, several inward routes may be exploited by ectodermal cells, leading to AuNP internalization, illustrated on the left panel: (i) direct membrane translocation, (ii) loading on nanovesicles, (iii) endocytosis (macropynocytosis) through large membrane invaginations. These processes occur within 30 min to 24 h, when a massive recruitment of particles from different cytoplasmic districts into vesicle/vacuole structures is observed. From 24 to 48 h a dynamic exchange of particles between different cell compartments (late endosome/phagosome-lysosome) takes place and AuNPs appear also to move out of vesicle membranes. After 48 h of incubation AuNPs are found at a great extent in lysosomes, but also on exosome-like vesicles. We suggest that following endosomal recruitment several outward routes may take place: (i) through exosomes (possibly derived by late endosomes), (ii) direct membrane exocytosis of NP-loaded vesicles, (iii) fusion of lysosomes with cell membrane. In the scheme the black and red arrows indicate the inward and outward routes, respectively, the dotted arrows indicate possible intracellular trafficking.

TABLE 2. ICP-AES (Inductively Coupled Plasma Atomic Emission Spectroscopy) Results[a]

time (h postwashing)	intracellular Au content (μg)	extracellular Au (μg)
0	93,74 ± 1.55	0
24	26,14 ± 1.20	0.819 ± 0.012
48	23,14 ± 0.42	0

[a] ICP-AES was performed on animals pulsed 24 h with 25nM AuNPs (corresponding to 1.25 mg), then washed and chased in fresh medium for 24 and 48 h. At each time point 150 animals (and 1 mL of their incubation medium) were collected and processed for ICP-AES. Experiments were performed in duplicate. Values are indicated as micrograms ± SE.

of the exocytosis, elemental analysis by mean of ICP-AES (inductively coupled plasma atomic emission spectroscopy) was performed on animals pulsed 24 h with 25 nM AuNPs (corresponding to 1.25 mg), then washed and chased in fresh medium for 24 and 48 h. The Au content (calculated on 150 treated animals) at the end of the pulse (24 h) was estimated as 93.7 μg, namely 7.5% of the total dose used for treatment. Following washing, the Au content decreased down to 26.1 and 23.1 μg, respectively at 24 and 48 h time points, indicating a 75% release of the internalized material. Interesting, this massive release occurred within the first 24 h of chasing, as after 48 h a quite similar Au value was measured. From analysis of the supernatants collected during the "chase" phase, low but detectable Au amounts (0.8 μg) were found only at 24 h postwashing, confirming AuNP exocytosis mainly occurring within this temporal window (see Table 2). Although the number of animals employed for the ICP was elevated (150), and the experiments were run in duplicate, the measure of Au content by ICP-AES produces an estimation of the general trend of the endocytosis/exocytosis, and the calculated gold amounts should not be considered as absolute to calculate the real extent of these processes. Overall these findings confirm the kinetics of AuNP entry/exit suggested by the TEM images: AuNPs are moderately recruited into vesicles within the first 24 h of incubation, and then sorted out (1) to lysosomes for external release during the following 24 h, (2) to more stable structures, possibly representing storage vacuoles, discharging their content over a longer period. The unavailability of molecular markers specific for *Hydra* storage/garbage vesicles makes it impossible to further characterize the nature of such structures.

CONCLUSIONS

The complexity of the molecular interactions underlying the endocytosis suggests that a great evolutionary effort has been spent to regulate the cellular response to a variety of different environmental stimuli. In multicellular organisms the endocytic and secretory pathways evolved to control all aspects of cell physiology and intercellular communication (immune response, development, hormone-mediated signal transduction, neurotransmission). Nanoparticles, being crystalline solids, can have inherently different properties from other molecules, which might dictate different mechanisms regarding transmembrane transport, intracellular sorting and excretion. While much of the knowledge regarding the cellular uptake and fate of gold nanoparticles has been acquired through *in vitro* cell culture studies, and relies on the response of single cells to AuNPs, here we captured these dynamics *in vivo*, on a simple animal structured as a living bilayered tissue, presenting physiological connections among all cells exposed to NPs. We present direct TEM evidence of several ongoing mechanisms underlying inward and outward trafficking of AuNP tailored with different molecules. The positive surface charge does control the early interaction with the cells, greatly enhancing the efficiency of uptake of AuNP-N_3 compared to AuNP-siRNA, while the mechanisms of uptake are shared by the two different functionalizations. Interestingly, beside expected endocytosis and macropynocytosis (trapping of large fluid pockets by formation and enclosure of membrane invaginations), we showed at least two unusual internalization routes: (1) direct membrane translocation for both AuNP-N_3 and AuNP-siRNA; (2) cell entry mediated by nanovesicles, enabled by the combination of the HP-TEM technique and the low AuNP concentrations. The nanovesicles may represent glycocalix structural components externally released (and thus NPs passively bind and follow the fate of such structures) or, alternatively, considering their size and morphology, they may represent exosomes, that is, endosomal-derived vesicles shipping extracellular messages, which may entrap AuNPs. The role of the exosomes in cell and animal physiology (immune response, cell signaling) has recently emerged,[35] thus their labeling with AuNPs may provide a unique tool to elucidate their biogenesis and fate. TEM imaging performed at 24 and 48 h time points showed several cell compartments containing the NPs, spanning from early- to late-endosomes, to lysosomes. In addition, AuNPs were found in the act of endosome escaping and traversing intracellular membranes (*i.e.*, AuNP-siRNA present on membranes of interstitial cells), depicting multiple highly dynamic processes elicited in response to AuNPs, over the first 24 h. The elemental analysis confirmed the kinetic of internalization and in addition showed that within 48 h, most of the internalized gold was cleared out the animal.

The dynamic and kinetic of the whole journey of gold nanoparticles within an animal, is here reported for the first time. On one hand, they perfectly mirror previous data obtained in mammalian cells, showing the conservation of such mechanisms throughout the animal kingdom, but, on the other hand, they extend the knowledge of new inward and outward mechanisms negotiating the entrance, trafficking,

and clearance of gold nanoparticles in animal cells. This may have a profound impact in the design of nanodevices for biomedical application and in basic cell biology.

MATERIALS AND METHODS

Nanoparticle Synthesis. Hydrogen tetrachloroaurate (III) hydrate ($HAuCl_4$) was supplied by Strem Chemicals, and *O*-(2-aminoethyl)-*O*′-(2-azidoethyl)pentaethylene glicol was supplied by Iris Biotech. Citrate, γ-tiobutirolactone, triethylamine, dimethyl sulfoxide, sodium dodecyl sulfate, and sodium hydroxide were purchased from Sigma-Aldrich.

Synthesis of Citrate-Gold Nanoparticles (Au NPs). Gold nanoparticles with an average diameter of ~14 nm were synthesized by the citrate reduction method as described.[26] Briefly, hydrogen tetrachloroaureate (III) hydrate (Strem Chemicals) (0.2 g; 0.589 mmol) was dissolved in 500 mL of Milli-Q water, heated, and stirred under reflux. When the solution boiled, sodium citrate dihydrate (0.598 g; 2.03 mmol) was added resulting in a red solution. The solution was kept under ebullition and protected from light for 30 min, and then cooled down and kept protected from light. The synthesized AuNPs were characterized by UV−vis due to its surface plasmon resonance (λ_{max}, 519 nm) and by transmission electron microscopy.

Synthesis of N-(20-azido-3,6,9,12,15,18-hexaoxoicosane)-4-mercaptobutanamide (HS-$(CH_2)_3$-CONH-EG(6)-$(CH_2)_2$-N_3). For the synthesis, 0.6 mmol of α-amine-ω-azido hepta(ethylene glycol) were added to 12.5 mL of dimethylsulfoxide under argon atmosphere in a poly(ethylene glycol) bath at 50 °C and under continuous stirring. Subsequently, 0.63 mmol of γ-tiobutirolactone and 5.7 mmol of triethylamine were added. After 5 h, the mixture was cooled down and lyophilized obtaining yellow oil. The yield of the reaction was 93%, without any further purification step. The product was characterized by FT-IR: 3301 cm^{-1} (NH st), 2870 cm^{-1} (−CH st), 2530 cm^{-1} (SH st), 2106 cm^{-1} (N_3 st), 1663 cm^{-1} (C═O st). ^{1}H-RMN 300 MHz (δ): 2,00 (m, 2H); 2,25 (t, 2H, J = 7,30 Hz); 2,65 (t, 2H, J = 7,00 Hz); 3,01 (s, 1H, SH); 3,32 (t, 4H, J = 5,00 Hz); 3,37 (t, 2H, J = 5,22 Hz); 3,59 (s, 22H); 6,60 (t, 1H, J = 4,76 Hz), and mass spectroscopy [M−H+], 451.1.

Functionalization of AuNPsAuNP-N_3. A AuNP solution (10.7 nM) and HS-$(CH_2)_3$-CONH-EG(6)-$(CH_2)_2$-N_3 (28 μM) was prepared the presence of SDS (0.028% v/v). NaOH was further added to a final concentration of 25 mM, and the mixture was incubated for 16 h at room temperature with strong stirring (it is important to follow this order of addition in order to avoid aggregation). The excess of PEGylated chain was washed away by centrifugation at 14000 rpm at 4 °C for 30 min times three. Z potential values for this sample provided a value of +21 mV (pH 7, 1 mM KCl). MALDI-TOF analysis confirmed the presence of PEG-N_3 ([M−H+], 451.1). The DLS measurement of AuNP-N_3 was 15.5 nm.AuNP-siRNA. AuNPs functionalized with HS-$(CH_2)_3$-CONH-EG(6)-$(CH_2)_2$-N_3, HS-EG(8)-$(CH_2)_2$−COOH, and siRNA were prepared following the protocols previously published.[25] Briefly, a mixture of 10 nM of citrate−gold nanoparticles, 7 μM SH-EG(8)-$(CH_2)_2$-COOH and 7 μM SH-$(CH_2)_3$-CONH-EG(6)-$(CH_2)_2$-N_3, and 0.028% SDS were prepared. NaOH was further added to a final concentration of 25 mM and the mixture was incubated for 16 h at room temperature. The excess of PEG chains was removed by centrifugation at 14.000 rpm for 30 min at 4 °C, and the supernatant was discarded. This washing process was repeated three times, and the pellet of AuNPs was dissolved in pure water.

For siRNA functionalization, the HS-siRNA previously treated with DTT and purified was incubated at a constant concentration of 5 nmol/mL with RNase free solution of AuNP previously functionalized with PEG (10 nM) containing 0.028% SDS (w/v). Subsequently, the salt concentration was increased to 0.1 M NaCl with brief ultrasonication following each addition to increase the coverage of oligonucleotides on the nanoparticle surface. Following 16 h incubation at 4 °C, the particles were purified by centrifugation at 14000 rpm 30 min at 4 °C and resuspended in DEPC-water 3 times.

The siRNA attached to the AuNP-siRNA was determined by quantification of the excess with the nucleic acid intercalator GelRed (Biotium), measuring its fluorescence at 602 nm. It was found that 41.3 ± 0.8 strands/AuNP were bound.

The sequence of the siRNA used targeting the *Hydra* myc 1 gene (Accession No. GQ856263) is as follows. Sense: 5′-thiol AAGAUGCUCACGCGUCAAGAAUU-3′. Antisense: 5′-UUCUUGACGCGUGAGCAUCUU-3′.

Animal Culturing and *in Vivo* Experiments. *Hydra vulgaris* (strain Zurich, originally obtained by P. Tardent), were cultured in *Hydra* medium (SolHy) comprising 1 mM $CaCl_2$, 0.1 mM $NaHCO_3$, pH 7.0, fed on alternate days with *Artemia nauplii* at 18 °C with 12:12 h light. Polyps from homogeneous populations, three weeks old, were selected for experiments, performed in an air-conditioned environment at 22 °C. The tests were initiated by collecting groups of 10 animals in plastic multiwells, followed by the addition of 70 nM AuNP (either AuNP-N_3 or AuNP-siRNA) in 300 μL of SolHy to each well and incubation for the necessary time periods. Nanoparticle uptake was monitored *in vivo* by a stereomicroscope (Olympus ZSXRFL2). Following extensive washes, *in vivo* imaging was accomplished by an inverted microscope (Axiovert 100, Zeiss) equipped with a digital color camera (Olympus, DP70). For imaging acquisition and analysis the software system Cell F (Olympus) was used. At the time indicated above, animals were taken and processed for TEM analysis.

***Hydra* Cell and Tissue Analysis.** *Hydra* polyps were macerated into a suspension of fixed single cells as reported.[37] Animals were anaesthetized in 2% urethane in SolHy for 2 min. The relaxed and elongated *Hydra* were fixed with Lavdowsky's fixative (ethanol/formaldehyde/acetic acid/water as 50:10:4:40), rehydrated, and mounted on microscope slides in glycerol 50% in PBS (8 g/L NaCl; 0.2 g/L KCl; 1.44 g/L $Na_2HPO_4 \cdot 7H_20$; 0.24 g/L KH_2PO_4).

Tissue sectioning: Treated animals were soaked overnight in 30% sucrose in PBS and then embedded in the frozen section medium Neg-50 (Richard-Allan Scientific). Cryosections of 10 μm thickness were obtained by a cryostat (Leitz, digital 1760), collected on adhesion microscope slides (SuperFrost Plus, Menzel) mounted in DAKO mounting medium (DAKO) or dehydrated in ethanol, equilibrated in xylene and mounted in D.P.X (Sigma) before imaging.

Transmission Electron Microscopy Analysis. Following exposure to nanoparticles, animals were extensively washed, then treated with 2% urethane in SolHy to prevent contraction and fixed for 2 h in 2% glutaraldehyde in SolHy. Samples were washed at least four times with SolHy and postfixed for 45 min with 1% buffered OsO_4. After a series of four washes in SolHy, animals were dehydrated in a graded ethanol series (30%, 50%, 70%, 90%, 100%), incubated 3 × 15 min with propylene oxide and then overnight in a 1:1 mixture of propylene oxide/Epon 12 resin. Before they wereflat embedded, the animals were incubated 2 × 2 h in Epon 12 resin. Serial thin sections (70 nm) prepared from animal tentacles and body regions below the head level were cut with a diamond knife and mounted onto 150−200 mesh Hex grids. Thin sections were stained with uranyl acetate and lead citrate. Ultrathin sections were examined with a Leo 912 AB transmission electron microscope operating at 80 kV.

Sample Preparation for High-Pressure Freezing Procedure (HPF). *Hydra* polyps immersed in SolHy were dissected into appropriate pieces to fit into cup-shaped HPF specimen carriers. Tissue pieces were pipetted with SolHy into a 0.2- or 0.3-mm deep carrier and covered with an additional carrier. Finally, the obtained sandwiches were cryo-immobilized by HPF. Frozen sandwiches were transferred into appropriate containers for storage in liquid N_2 for later use or subjected to freeze substitution (FS). The frozen samples were transferred under liquid N_2 into cryovials containing frozen FS cocktails (anhydrous acetone plus 1% OsO_4 and 0.1−0.2% uranyl acetate). Subsequently, the lids were screwed loosely onto the vials to permit safe evaporation of excess N_2 gas. The vials were placed into the precooled

FS device, and after about 1 h the lids were tightened and FS was performed for at least 8 h at −80 to −90 °C; warming up to −55 °C at a rate of 5−10 °C per hour, subsequent postfixation and staining at −55 °C for 6 h, followed by warming up to −30 °C at a rate of 5−10 °C per hour where samples were left for an additional 3 h.[38] Finally the samples were washed 3× with acetone (10 min each), 16 h in 10% epoxy resin (Epon) in acetone, 6 h in 30% Epon in acetone, 16 h in 70% Epon in acetone, 6 h in 100% Epon in acetone, and finally 16 h in 100% Epon in acetone. Then the samples were placed in fresh resin and placed in an oven at 60 °C overnight.

Sample serial thin (70 nm) sections of tentacles and body regions were cut with a diamond knife and mounted onto 150−200 mesh Hex grids. Ultrathin sections were examined with transmission EM Libra 120 EFTEM (Zeiss, Oberkochen, Germany) at 80 eV.

Elemental Analysis by Inductively Coupled Plasma Atomic Emission Spectroscopy (ICP-AES). To estimate the extent of endocytosis and exocytosis of AuNP-N_3 in *Hydra*, living polyps were treated 24 h with AuNP, washed, and processed for elemental analysis to evaluate the amount of Au present inside the animals and released in the medium. A total of 1500 *Hydra* polyps were incubated in 3 mL of SolHy with 25 nM AuNP-N_3 for 24 h. At this time point 150 polyps were extensively rinsed and homogenized for ICP-AES. The remaining animals were kept in fresh medium and saved at 24 and 48 h postwashing. For each time point the same amount of polyps (150) and incubation media were saved. Experiments were done in duplicate. For ICP-AES measurements, all the samples were treated with 400 μL of aqua regia overnight and then diluted with Milli-Q water to 20 mL to reach a final concentration of acid 2% (v/v).

Conflict of Interest: The authors declare no competing financial interest.

Acknowledgment. For financial support the authors thank FP7- NanoSciEraNet project NANOTRUCK, and ARAID (Spain). A.A. and V.M. were granted by NANOTRUCK, European Social Fund. Moreover, the authors thank G. Marino for technical support with *Hydra* culturing, Stazione Zoologica Anton Dohrn (Napoli) for access to TEM facilities; Michael W. Hess (Division of Histology and Embryology, Innsbruck Medical University) for providing the cryo-EM facility, and Karin Gutleben for excellent technical assistance. Authors thank Joao Conde and all NANOTRUCK members for all technical support and fruitful discussions.

Supporting Information Available: Long-term toxicity effects of AuNP in *Hydra*, additional TEM images supporting the mechanisms proposed for endocytosis, intracellular trafficking, and exocytosis of gold nanoparticles. This material is available free of charge *via* the Internet at http://pubs.acs.org.

REFERENCES AND NOTES

1. Conner, S. D.; Schmid, S. L. Regulated Portals of Entry into the Cell. *Nature* **2003**, *422*, 37–44.
2. Piper, R.; Katzmann, D. Biogenesis and Function of Multivesicular Bodies. *Annu. Rev. Cell Dev. Biol.* **2007**, *23*, 519–566.
3. Farokhzad, O.; Langer, R. Nanomedicine: Developing Smarter Therapeutic And Diagnostic Modalities. *Adv. Drug Delivery Rev.* **2006**, *58*, 1456–1465.
4. Hu, Y.; Fine, D. H.; Tasciotti, E.; Bouamrani, A.; Ferrari, M. Nanodevices in Diagnostics. *Wiley Interdiscip. Rev.* **2011**, *3*, 11–32.
5. Wang, A.; Langer, R.; Farokhzad, O. Nanoparticle Delivery of Cancer Drugs. *Annu. Rev. Med.* **2012**, *63*, 185–283.
6. de la Fuente, J. M.; Berry, C. C. TAT Peptide as an Efficient Molecule to Translocate Gold Nanoparticles into the Cell Nucleus. *Bioconjugate Chem.* **2005**, *16*, 1176–1180.
7. Ruoslahti, E. Peptides as Targeting Elements and Tissue Penetration Devices for Nanoparticles. *Adv. Mater.* **2012**, *24*, 3747–3756.
8. Child, H. W.; Del Pino, P. A.; de la Fuente, J. M.; Hursthouse, A. S.; Stirling, D.; Mullen, M.; Mcphee, G. M.; Nixon, C.; Jayawarna, V.; Berry, C. C. Working Together: The Combined Application of a Magnetic Field and Penetratin for the Delivery of Magnetic Nanoparticles to Cells in 3D. *ACS Nano* **2011**, *5*, 7910–7919.
9. Bartczak, D.; Nitti, S.; Millar, T. M.; Kanaras, A. G. Exocytosis of Peptide Functionalized Gold Nanoparticles in Endothelial Cells. *Nanoscale* **2012**, *4*, 4470–4472.
10. Jiang, X.; Rocker, C.; Hafner, M.; Brandholt, S.; Dorlich, R. M.; Nienhaus, G. U. Endo- and Exocytosis of Zwitterionic Quantum Dot Nanoparticles by Live HeLa cells. *ACS Nano* **2010**, *4*, 6787–6797.
11. Chithrani, D. B. Intracellular Uptake, Transport, and Processing of Gold Nanostructures. *Mol. Membr. Biol.* **2010**, *27*, 299–311.
12. Giljohann, D. A.; Seferos, D. S.; Daniel, W. L.; Massich, M. D.; Patel, P. C.; Mirkin, C. A. Gold Nanoparticles for Biology and Medicine. *Angew. Chem., Int. Ed.* **2010**, *49*, 3280–3294.
13. Kim, C.-k.; Ghosh, P.; Rotello, V. Multimodal Drug Delivery Using Gold Nanoparticles. *Nanoscale* **2009**, *1*, 61–68.
14. Lin, J.; Zhang, H.; Chen, Z.; Zheng, Y. Penetration of Lipid Membranes by Gold Nanoparticles: Insights Into Cellular Uptake, Cytotoxicity, and Their Relationship. *ACS Nano* **2010**, *4*, 5421–5429.
15. Verma, A.; Stellacci, F. Effect of Surface Properties on Nanoparticle−Cell Interactions. *Small* **2010**, *6*, 12–21.
16. Oh, E.; Delehanty, J.; Sapsford, K.; Susumu, K.; Goswami, R.; Blanco-Canosa, J.; Dawson, P.; Granek, J.; Shoff, M.; Zhang, Q.; *et al*. Cellular Uptake and Fate of PEGylated Gold Nanoparticles Is Dependent on Both Cell-Penetration Peptides and Particle size. *ACS Nano* **2011**, *5*, 6434–6448.
17. Tortiglione, C. An ancient model organism to test in vivo novel functional nanocrystals In *Biomedical Engineering: From Theory to Application*; Fazel-Rezai, R., Ed.; InTech−Open Access Publisher: New York, 2011; Chapter 10.
18. Ambrosone, A., Tortiglione, C. Methodological Approaches for Nanotoxicology Using Cnidarian Models. *Toxicol. Mech. Methods* **2013** (in press) doi:10.3109/15376516.2012.747117).
19. Bottger, A.; Hassel, M. *Hydra*, a Model System to Trace the Emergence of Boundaries in Developing Eumetazoans. *Int. J. Dev. Biol.* **2012**, *56*, 583–91.
20. Ambrosone, A.; Mattera, L.; Marchesano, V.; Quarta, A.; Susha, A. S.; Tino, A.; Rogach, A. L.; Tortiglione, C. Mechanisms Underlying Toxicity Induced by CdTe Quantum Dots Determined in an Invertebrate Model Organism. *Biomaterials* **2012**, *33*, 1991–2000.
21. Tino, A.; Ambrosone, A.; Mattera, L.; Marchesano, V.; Susha, A.; Rogach, A.; Tortiglione, C. A New *in Vivo* Model System to Assess the Toxicity of Semiconductor Nanocrystals. *Int. J. Biomater.* **2011**, 792854.
22. Tortiglione, C.; Quarta, A.; Malvindi, M. A.; Tino, A.; Pellegrino, T. Fluorescent Nanocrystals Reveal Regulated Portals of Entry into and between the Cells of *Hydra*. *PLoS One* **2009**, *4*, e7698.
23. Malvindi, M. A.; Carbone, L.; Quarta, A.; Tino, A.; Manna, L.; Pellegrino, T.; Tortiglione, C. Rod-Shaped Nanocrystals Elicit Neuronal Activity *in Vivo*. *Small* **2008**, *4*, 1747–1755.
24. Ambrosone, A.; Marchesano, V.; Tino, A.; Hobmayer, B.; Tortiglione, C. Hymyc1 Downregulation Promotes Stem Cell Proliferation in *Hydra* Vulgaris. *PLoS One* **2012**, *7*, e30660.
25. Conde, J.; Ambrosone, A.; Sanz, V.; Hernandez, Y.; Marchesano, V.; Tian, F.; Child, H.; Berry, C. C.; Ibarra, M. R.; Baptista, P. V.; Tortiglione, C.; De La Fuente, J. M. Design of Multifunctional Gold Nanoparticles for *in Vitro* and *in Vivo* Gene Silencing. *ACS Nano* **2012**, *6*, 8316–8324.
26. Hartl, M.; Mitterstiller, A. M.; Valovka, T.; Breuker, K.; Hobmayer, B.; Bister, K. Stem Cell-Specific Activation of an Ancestral Myc Protooncogene with Conserved Basic Functions in the Early Metazoan *Hydra*. *Proc. Natl. Acad. Sci. U.S.A.* **2010**, *107*, 4051–4056.
27. Turkevich, J.; Stevenson, P. C.; Hillier, J. A Study of the Nucleation and Growth Processes in the Synthesis of Colloidal Gold. *Discuss. Faraday Soc.* **1951**, *11*, 55–75.
28. Ojea-Jimenez, I.; Puntes, V. Instability of Cationic Gold Nanoparticle Bioconjugates: The Role of Citrate Ions. *J. Am. Chem. Soc.* **2009**, *131*, 13320–13327.

29. Krpetic, Z.; Porta, F.; Caneva, E.; Dal Santo, V.; Scari, G. Phagocytosis of Biocompatible Gold Nanoparticles. *Langmuir* **2010**, *26*, 14799–14805.
30. Verma, A.; Uzun, O.; Hu, Y.; Hu, Y.; Han, H. S.; Watson, N.; Chen, S.; Irvine, D. J.; Stellacci, F. Surface-Structure-Regulated Cell-Membrane Penetration by Monolayer-Protected Nanoparticles. *Nat. Mater.* **2008**, *7*, 588–95.
31. Ding, H. M.; Ma, Y. Q. Interactions between Janus Particles and Membranes. *Nanoscale* **2012**, *4*, 1116–1122.
32. Bottger, A.; Doxey, A. C.; Hess, M. W.; Pfaller, K.; Salvenmoser, W.; Deutzmann, R.; Geissner, A.; Pauly, B.; Altstatter, J.; Munder, S.; *et al*. Horizontal Gene Transfer Contributed to the Evolution of Extracellular Surface Structures: The Freshwater Polyp *Hydra* Is Covered by a Complex Fibrous Cuticle Containing Glycosaminoglycans and Proteins of the PPOD and SWT (Sweet Tooth) Families. *PLoS One* **2012**, *7*, e52278.
33. Krpetic, Z.; Saleemi, S.; Prior, I.; See, V.; Qureshi, R.; Brust, M. Negotiation of Intracellular Membrane Barriers by TAT-Modified Gold Nanoparticles. *ACS Nano* **2011**, *5*, 5195–5396.
34. Andrews, N. Regulated Secretion of Conventional Lysosomes. *Trends Cell Biol* **2000**, *10*, 316–321.
35. Keller, S.; Sanderson, M.; Stoeck, A.; Altevogt, P. Exosomes: From Biogenesis and Secretion to Biological Function. *Immunol. Lett.* **2006**, *107*, 102–108.
36. Record, M.; Subra, C.; Silvente-Poirot, S.; Poirot, M. Exosomes as Intercellular Signalosomes and Pharmacological Effectors. *Biochem. Pharmacol.* **2011**, *81*, 1171–1182.
37. David, C. N. A Quantitative Method for Maceration of *Hydra* Tissue. *Wilhelm Roux Arch.EntwMech. Org.* **1973**, *171*, 259–268.
38. Holstein, T.; Hess, M.; Salvenmoser, W. Preparation Techniques for Transmission Electron Microscopy of *Hydra*. *Methods Cell Biol.* **2010**, *96*, 285–591.